Wenbiao Han

Mohsen A. Jafari*

Department of Industrial & Systems Engineering,
Rutgers University,
96 Frelinghuysen Road,
Piscataway, NJ 08854

Stephen C. Danforth

Ahmad Safari

Department of Ceramic & Materials Engineering,
Rutgers University,
607 Taylor Road,
Piscataway, NJ 08854

Tool Path-Based Deposition Planning in Fused Deposition Processes

The fabrication of a functional part requires very high layer quality in the Fused Deposition (FD) processes. The constant deposition flow rate currently used in FD technology cannot meet this requirement, due to the varying geometries of the layers. To achieve a high quality functional part, an overfill and underfill analysis is conducted. A deposition planning approach is proposed, which is based on a grouping and mapping algorithm. Two piezoelectric test parts have been built to demonstrate the effectiveness and feasibility of the proposed approach. [DOI: 10.1115/1.1455026]

1 Introduction

Layered manufacturing (LM) enables a dramatic reduction in the lead time and the cost of part design and manufacturing in contrast to traditional manufacturing techniques. The application of LM processes are being extended from conceptual prototype modeling to advanced functional part building. In the fused deposition (FD) based LM processes, FD modeling (FDM) is extended to FD of ceramics (FDC) [1], FD of multiple materials (FDMM) [2] and FD of metals (FDMet) [3]. FDC and FDMM are employed to make functional ceramic components such as turbine components, high authority actuators and novel structured piezoelectric transducers/sensors [2,4,5]. FDMet is applied to build metallic components, e.g. hard tooling with stainless steel [6]. There is an ever-increasing demand for building parts with improved quality, tolerance and surface finish.

The main quality requirements for parts usually refer to surface roughness, dimensional accuracy, and part strength [7]. In general, a functional part needs more strict requirements than prototypes. Layer quality, quantified by the amount of overfills, underfills, and contour dimensions, which is not so important in prototype modeling, is critical for building functional ceramic components [8]. Layer defects are difficult, if not impossible, to be compensated for in post-deposition processes. Hence, layer quality deserves more attention during green part construction. For structural applications, a functional part requires significant strength and stiffness when undertaking a real task, e.g. tooling [9].

A number of factors contribute to part quality (mentioned above) in the FD processes. For surface roughness these factors are layer thickness [10], part orientation [11], material properties [12], temperature [13], and some process parameters such as nozzle size, etc. For dimensional accuracy the controlling parameters are CAD model representation (tessellated vs. parametric surface) [10], path tracking accuracy [14], interpolation method (linear vs. miscellaneous), and deposition flow rate. For part strength the factors are fill pattern and vector angle [15], temperature profile [16], and material characteristics. Layer quality is reflected by the difference between the designed part and the built part, i.e. the amount of excess (overfilled) or insufficient (underfilled) material deposited, assuming that the part is well designed. We refer to the condition of overfills (bumps or excess material) and underfills (gaps or voids) in a layer as *layer evenness*, which is determined by tool path, positioning precision, deposition accuracy, and materials as well as some process parameters.

Although the studies of these contributory factors have led to a variety of methods to improve part quality, there are fundamentally three approaches (see Fig. 1): (1) CAD model optimization according to certain objectives, including part orientation, support structure generation and slicing [17]. Part orientation can be selected based on certain criteria, e.g. minimum build height, minimum support volume, etc. [11]. An acceptable surface smoothness (staircase effect) can be achieved for an analytical surface through variable thickness slicing, while both layer amount and building time are reduced [10]. (2) Layer interior planning. This includes tool path generation/optimization, deposition planning, and selection of process parameters. To obtain required part stiffness, a specific deposition strategy can be chosen in terms of fill patterns (contours, vectors, and spirals) and vector angles (-180 deg ~ 180 deg) [15]. The proper selection of tool path pattern may ensure both surface finish and part strength [18]. It is suggested that contour filling be used for the part boundaries for achieving good surface smoothness and vector filling be used for the interior regions of the part for achieving required part strength. Shape optimization may remove or minimize gaps or path discontinuities using adaptive offset fill pattern [19]. Void quantification based on designed filling path [20] is helpful in optimizing tool path. (3) On-line monitoring and control of FD process. This includes three key aspects, i.e. precise positioning of the X-Y-Z table, flow control, and defect detection during part building. A trajectory planning scheme was proposed in [14] to reduce path tracking errors under the constraint that the liquifier head must move with constant speed as much as possible. Jafari et al. have developed a novel system for Fused Deposition of Multiple Materials (FDMM) to fulfill all three aspects in monitoring and controlling of the FDC, FDMM, and FDMet processes [2].

This article addresses issues encountered in deposition planning of the FD processes. Although the geometric complexity of a part has been reduced dramatically via slicing, its planar geometric and topological complexity still significantly affects the building process. Usually, in order to obtain a desirable layer quality, an operator of an FD machine for ceramics and metals has to keep observing the build process and modify the process parameters, e.g. speed of the roller that drives the filament, in order to compensate manually for the overfills and underfills within each layer. Assuming a negative offset design, if overfill (underfill) is observed, the roller speed must be reduced (increased) in order to decrease (increase) flow rate. The more complex the part geometry, the more frequently the operator must make such adjustments. In the FD processes, layer evenness of the current layer is strongly correlated to its two adjacent layers. If the previous layer is overfilled (underfilled), the current layer is very likely to be
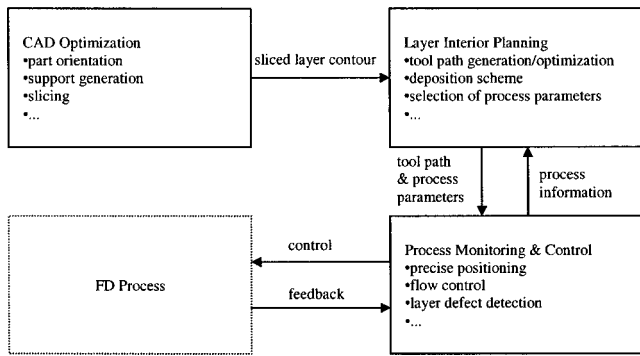

Fig. 1 Approaches for improving part quality in the FD processes

Fig. 2 Terminology in vector fill pattern

overfilled (underfilled), and this will continue if the process parameters are kept constant. If the part geometry varies from layer to layer, it will be more difficult for an operator to properly change the process parameters and it will be very hard to make a functional part of acceptable quality in a few runs and in a short time.

To further upgrade FD automation and build advanced functional ceramic and metallic parts of high quality in a more efficient way, we studied the causes of overfills/underfills as well as the relationship between the planar geometric complexity of a layer and the overfill/underfill phenomena. As a result, we propose a grouping and mapping algorithm based on tool path, in which adjacent vector segments with similar lengths are grouped together. A deposition flow rate is then assigned to each group, according to the mean value of the vector segment lengths in that group using linearized mapping functions.

The remainder of this article is organized as follows. An analysis of the overfill and underfill phenomena in the FD processes is conducted in section 2. Section 3 presents the proposed grouping and mapping algorithm. The implementation issues and manufacturing examples are given in section 4 to demonstrate the feasibility of the proposed approach. We conclude this article and address future research in section 5.

2 Analysis of Overfill and Underfill in the FD Processes

2.1 FD Technique Description. The FD technique shares the common procedures as other LM techniques. In sequence, they are CAD model design, tessellated format generation, slicing and tool path generation. The original CAD model can also be sliced directly without surface tessellation [21]. In the FD technique, the usually applied layer filling strategies are: (1) The boundaries use contour filling and the interiors use vector filling; (2) The contour is laid down first, after which the interior is filled; (3) The offset (distance between roads) between a vector and a contour is negative; (4) The vector angle is alternated by 90 degrees between consecutive layers. Vector is the most frequently used fill pattern, which consists of a series of vector segments (along the vector angle) connected by small turn segments (see Fig. 2). The unique aspects of the FDC, FDMM and FDMet techniques lie in the materials, the fabrication process, and the post processing (binder removal, sintering) [2,6,12]. In this article, we will focus on the fabrication process of the green parts, which is illustrated in Fig. 3. A FD machine consists essentially of a material deposition subsystem, which consists of one (or multiple) driver-liquefier(s) (we call it *head* thereafter) attached to a carriage and their controllers, and a positioning subsystem, which consists of the X-Y-Z table and its controller that enables the carriage to move in the horizontal X-Y plane and a fabrication platform to move in the Z direction [2,13]. The function of the
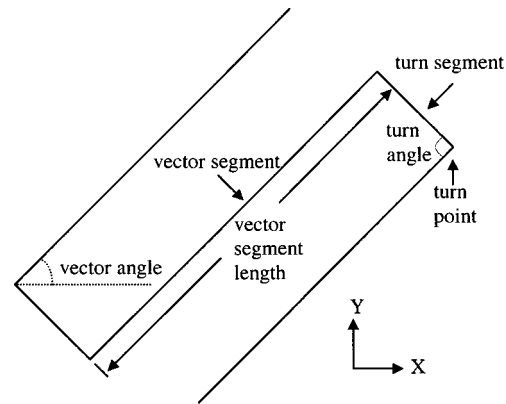
driver-liquefier is to pump the (ceramic, metallic, fugitive) filament into the heated liquefier through a pair of motor driven rollers and extrude the semi-solid material through the nozzle onto the build platform following the designed tool path. There is a shearing effect that forces material to spread forwards and sidewards when the nozzle moves. Once a layer is built, the platform goes down a distance of the layer thickness (along the Z direction) and the following layer is deposited on top of the previous one. In the following sections, we will conduct an overfill and underfill analysis. Unless mentioned otherwise, all the effects related to overfills and underfills are in-plane ones.

2.2 Overfill and Underfill Analysis. According to the mass balance principle, assuming the process is in steady state, we have

$$m_{\mathrm{in}} = m_{\mathrm{out}} \qquad (1)$$

where m_{in} (kg/s) is the mass of the filament driven to the liquefier in a unit time, m_{out} (kg/s) is the mass of the semi-solid material flowing out of nozzle in a unit time. Further, we have

$$S_{\mathrm{road}} = K \cdot \frac{V_{\mathrm{roller}} S_{\mathrm{filament}}}{V_{\mathrm{head}}} \qquad (2)$$

where $K = \rho_{\mathrm{in}} / \rho_{\mathrm{out}}$ is a constant, ρ_{in} and ρ_{out} are the densities of solid filament and semi-solid material respectively, V_{roller}(m/s) is the roller speed, V_{head}(m/s) is the head motion speed, S_{filament}(m^2) and S_{road}(m^2) are the cross sectional areas of the filament and the deposited road respectively (see Fig. 4).

To avoid overfills and underfills due to improper (or lack of) control of the FD process in a layer, we must fix the cross section geometry of deposited roads complying with the designed values,
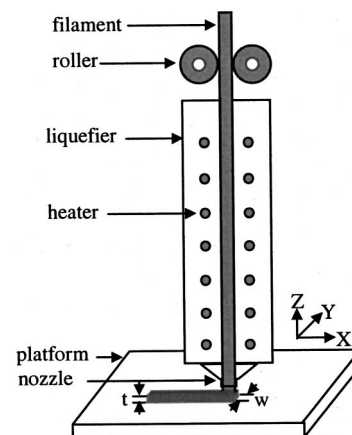

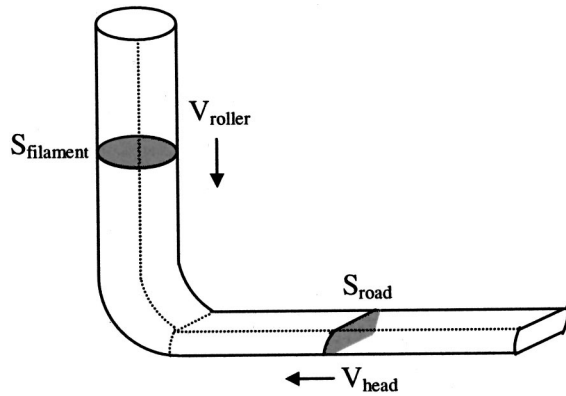**Fig. 3 Schematic of fused deposition process**

Fig. 4   Schematic of steady deposition state

Fig. 6   Actual tool path vs. head speed (sample period = 10 ms)

i.e. S_{road} needs to be kept constant. Since S_{filament} is constant (with a small variance) in Eq. (2), it is necessary and sufficient to keep S_{road} constant by keeping constant the ratio between V_{roller} and V_{head}. However, due to process characteristics, this ratio is always changing if no control or deposition planning is involved. The next section will explore this issue in detail.

2.2.1 Overfills Due to Decrease of Head Speed at Turns. The most frequently used fill pattern in the FD processes is vector, which is used to fill internal areas of closed boundaries. A vector is discontinuous at turn points. This means that the deposition head always undergoes acceleration and deceleration at these locations. In practice, usually two schemes can be applied for changing the speed at turns [22]. One is to decelerate the X-Y table to zero speed at the turn point and accelerate to the predefined speed from the turn point, so-called *stop-at-turn* scheme. The other is to blend smoothly from the speed for the first move to the speed for the second move according to the predefined acceleration/deceleration parameters, so-called *blended-move* scheme. Since X-Y table moves in a coordinated fashion, two axes will accelerate and decelerate synchronously, i.e. their acceleration or deceleration times (T) are equal to each other. Furthermore, reference acceleration or deceleration of each axis remains constant during speed change within time T, but they may change from time to time depending on the initial speed and ending speed in a speed change. A blended move is illustrated in Fig. 5, where point A and point B are the locations that a blended move starts and ends respectively. Corresponding to these two speed change schemes at turns, we have the following three properties:

Property 1: *When the X-Y table moves along a vector with a constant velocity, it cannot exactly follow the tool path at a turn unless it decelerates to zero at the turn point.*

Property 2: *In a vector movement, if the X-Y table moves at constant velocity V_0 along a continuous line and makes a blended move at a turn, its velocity during the turn period T is always less than V_0. The more acute the turn angle is, the more speed reduction occurs during the turn.*
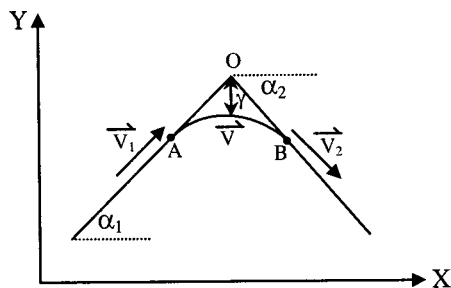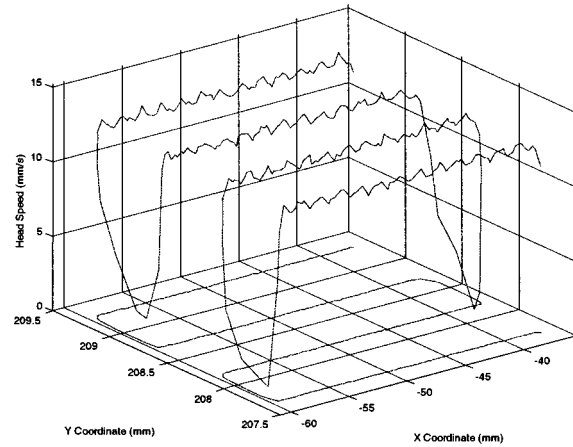

Fig. 5   Speed change at a turn point

Property 3: *For a stop-at-turn scheme, let point A be the point where the motion along the first vector segment starts to decelerate to a stop (using T time) at the turn point, and point B be the point where the motion along the second vector segment completes acceleration from a stop at the turn point to the predefined speed (using T time). If a blended move starts at point A, then it ends at point B using T time.*

The proofs of Property 2 and 3 are given in the appendix. To exactly follow the tool path without stopping at a turn requires an infinite torque, which cannot be provided by the X-Y table. Therefore, the X-Y table has to stop at each turn in order to achieve exact positioning as Property 1 indicates. However, a stop-at-turn scheme may dramatically reduce the average table speed, especially for short segment length vectors. On the other hand, a blended-move scheme has less effect on the average table speed. Although it may introduce positioning errors at turns (e.g. γ in Fig. 5), according to Property 3, as long as the acceleration or deceleration period T is small and table speed is not high (which is true for FD techniques), the positioning errors at turns will remain in an acceptable range. Here, we select the blended-move scheme.

A tool path (vector) and the corresponding table speed are sampled from the FDMM system (see Fig. 6). In Fig. 6, the actual tool path is shown in the X-Y plane while the head speed is shown in the Z axis. This verifies Property 2 above. Property 1 and 2 indicate that regardless of the scheme, the X-Y table speed will drop down at turns. According to Eq. (2), if the roller speed remains constant (a usual case in current technology), the cross sectional area of a road will be increased. In addition, according to Property 2, if a blended-move scheme is used, the more acute the turn angle, the more the cross sectional area of a road is increased.

2.2.2 Overfills and Underfills Due to Vector Geometry at Turns. At a certain area near turn points, the material is deposited twice. This is illustrated in Fig. 7, where W is the road width and θ is the turn angle. Since γ is small in a blended move (see Fig. 5), we ignore it in our analysis. Note that the double deposition at turn points is different than what occurs in adjacent roads (of the negative offset) because the latter is made intentionally, while the former is unavoidable. Overfills always occur at turns.

Property 4: *Double deposition area (DDA) of a vector at a turn point increases when the turn angle decreases. DDA reaches a minimum when the turn angle $\theta = \pi$, and a maximum when $\theta = 0$. DDA is proportional to W^2 for a specific θ.*

The proof of Property 4 is shown in the appendix. The overfills from the vector geometry are significant when the vector consists of many short segments. In addition, overfills increase (decrease) when the road width is increased (decreased). Due to vector geometry, underfills might also occur at turns (see Fig. 7) [15]. These underfill areas are usually compensated for via the negative offset between contour filling and vector filling. The shearing ef-
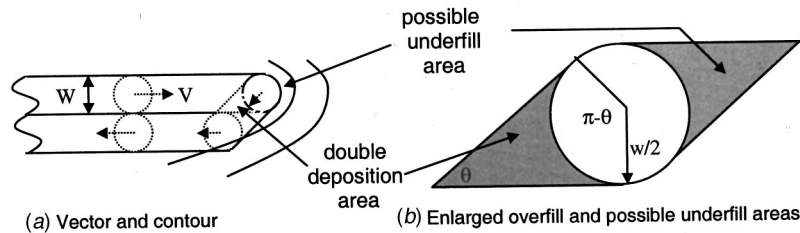
(a) Vector and contour

(b) Enlarged overfill and possible underfill areas

Fig. 7 Overfills and underfills due to vector geometry

fect of the nozzle will bring (excess) material from neighboring areas to fill those underfill areas. Hence, the underfills at turns can be removed via a careful tool path design, while overfills at turns are inevitable.

2.2.3 Overfills and Underfills Due to Inappropriate Road Width or Offset. When layer deposition is completed, two typical defects may be observed, i.e. gaps or voids (underfills) and bumps (overfills) between two adjacent roads. To study road geometry, we carried out experiments to create roads with different offsets. According to the cross section images of roads shown in Fig. 8, with a certain tolerance, we model road geometry along a straight path segment as in Fig. 9. The cross section geometry along the moving direction is a rectangle plus two semi-circles with the layer thickness t as its diameter. The road width in this geometry model is w.

To obtain an even layer surface, two adjacent roads must overlap (see Fig. 8 and Fig. 10). The currently depositing road will interact with the (already deposited) adjacent road to fill up the empty spaces. Figure 10 illustrates that the excess material in the common deposition area (S_1) will compensate for the empty spaces above and below the semi-circles (S_2 and S_3), i.e. we must have $S_1 = S_2 + S_3$, assuming the semi-solid material is incompressible.

Property 5: *In Fig. 10, to compensate for the empty spaces above and below the semicircles, the necessary negative offset f^* between two adjacent roads is $(\pi-4)t/4$.*

The proof of Property 5 is shown in the appendix. From Property 5 we know that the desired negative offset (f^*) is only a function of layer thickness (t). In FDC, FDMM, and FDMet processes, for a 250 μm slice thickness, the designed negative offset is usually chosen as 50 μm or 75 μm. According to Property 5, f^* should be 54 μm. This result conforms to the offset often chosen by experienced operators. Both gaps and bumps between two neighboring roads are supposed to be eliminated according to Property 5. A gap between two adjacent roads is depicted in Fig. 11, in which w_1 is the current road width, f_1 is the gap between roads, and l_1 is the interval between two designed tool paths. An overfill between two adjacent roads is depicted in Fig. 12, in which w_2 is the current road width, f_2 is the negative offset, and l_2 is the interval between two designed tool paths. To obtain an even layer surface,

we have two rules for adjusting road width or offset as follows: (1) When a gap between two adjacent roads occurs, it is sufficient to either increase the road width from $w_1 = l_1 - f_1 - t$ to $w_1^* = l_1 - f^* - t$ or decrease the distance between two roads, l_1, to $l_1^* = w_1 + t + f^*$ to attain the desired layer evenness as shown in Fig. 10. (2) When a bump between two adjacent roads occurs, it is sufficient to either decrease the road width from $w_2 = l_2 - f_2 - t$ to $w_2^* = l_2 - f^* - t$ or increase the distance between two roads, l_2, to $l_2^* = w_2 + t + f^*$ to attain the desired layer evenness as shown in Fig. 10.

Increasing (decreasing) the road width implies enlargement (reduction) of the cross sectional area of a road. According to Eq. (2), we must either increase (decrease) roller speed or decrease (increase) head speed. Decreasing l_1 (increasing l_2) implies that the tool path must be re-planned.

2.2.4 Overfills and Underfills Due to Other Reasons. Overfills and underfills can be caused by alternation of the vector angle. Due to Property 2 and 4, the following observation is easy to make: the longer (shorter) the vector segment length, the less (more) the overfill effect due to the reduced (increased) frequency of turns. Because of the non-uniform feature of part geometry along different vector angles, the vector segments that cover a certain area may be short (long) in one layer but long (short) in the next layer. If a certain value of flow rate is appropriate for one area covered by short (long) vector segments, it may cause underfills (overfills) in the same area for the next layer. This phenomenon is illustrated via Fig. 13. Both rectangular parts have the sizes of 19.05 mm by 10.16 mm. In the previous layer, both parts have an even layer surface and a vector angle of 90 degrees. In the current layer, the vector angle becomes 0 degrees. The previous layer has shorter vector segment lengths than the current layer. Part 13a uses a larger flow rate than that used in the previous layer, while part 13b uses the same flow rate. The result is that part 13a still has an even layer surface (because the effect of increased vector segment lengths in the current layer is compensated by the increased flow rate), while part 13b is significantly underfilled.

The overfill and underfill condition in one layer is correlated with that in its two adjacent layers. If overfills (underfills) occur in
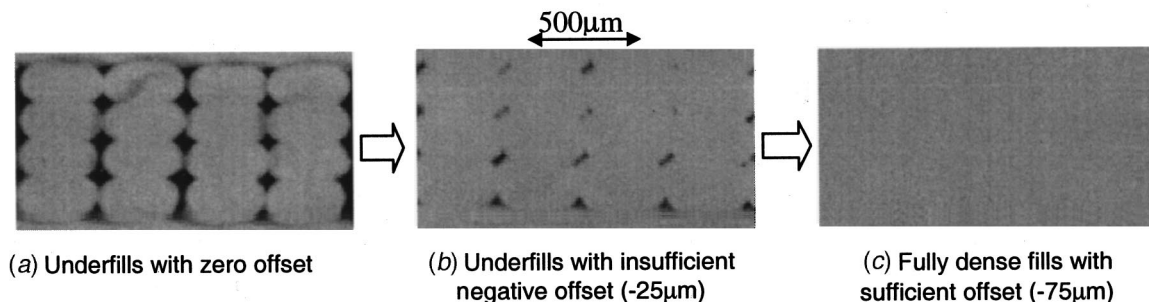

(a) Underfills with zero offset

(b) Underfills with insufficient negative offset (-25μm)

(c) Fully dense fills with sufficient offset (-75μm)

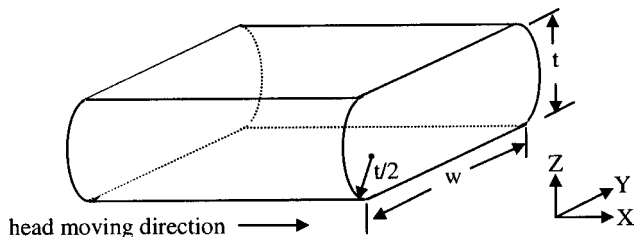**Fig. 8   Cross section images of road geometry under different offsets**

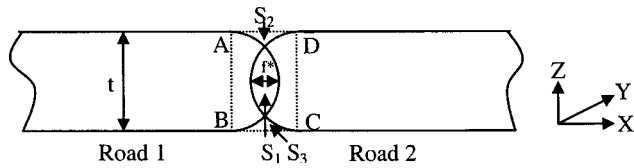**Fig. 9   Modeled deposition road geometry**

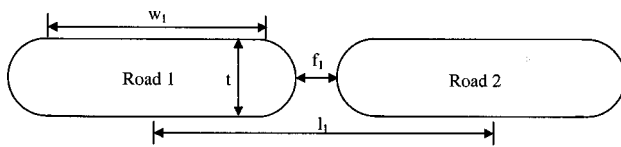**Fig. 10   Desired deposition with offset f***

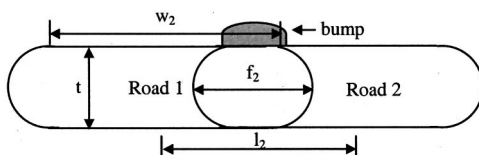**Fig. 11   Gap between two adjacent roads**

Fig. 12   Bump between two adjacent roads
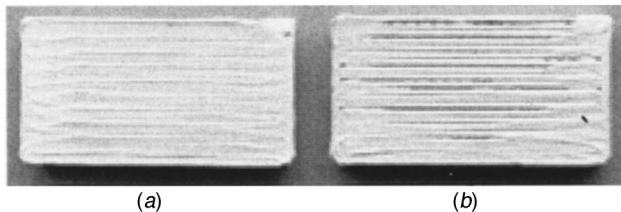

Fig. 13   Underfills due to change of vector angle (*a*) even layer of part 13a (*b*) underfilled layer of part 13b
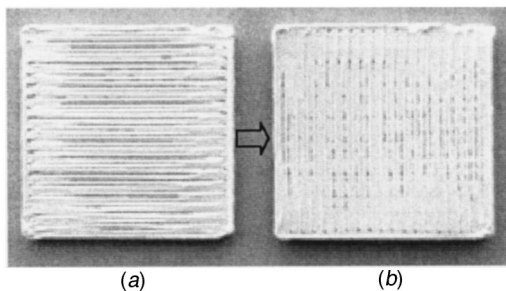

Fig. 14   Underfill correlation between two adjacent layers (*a*) current layer of part 14a (*b*) next layer of part 14b

an area of the current layer, and the same area in the next layer is covered by vector segments that are the same length as or shorter (longer) than those in the current layer, the overfill (underfill) condition in that area of the next layer will either not change or it will become worse due to material accumulation (insufficiency).

This phenomenon is demonstrated in Fig. 14 and Fig. 15 through four test parts. Each test part has a square layer with dimensions of 19.05 mm by 19.05 mm, i.e. each layer has an uniform vector segment length. Each part has an even layer surface in the previous layer. Part 14b (part 15b) has the same layer surface in the current layer as part 14a (part 15a). On the one hand, the flow rate is decreased in the current layer for part 14a and keeps the decreased value in the next layer for part 14b. On the other hand, the flow rate is increased in the current layer for part 15a and keeps the increased value in the next layer for part 15b. These tests show that underfills or overfills generated in the current layer may lead to (more) underfills or overfills in the next layer, if the flow rate is kept constant. This will continue such that the part becomes more and more underfilled or overfilled in the subsequent layers.

3   Deposition Planning

3.1   Preliminary Remarks.   Layer interior planning should consist of both tool path planning and deposition planning. Current FD technology only considers the former. Since the FD processes depend on both the positioning of the head and the deposition of material, planning without regard to deposition process is not complete and will not ensure a good quality of the functional part.

Since most of the areas within a layer are filled by the vector pattern according to the common deposition strategy in FDC, FDMM, and FDMet, our planning task will target this specific fill pattern. Complex geometry and topology within a layer usually lead to frequent changes of vector segment lengths, as shown in Fig. 17. One common case is that the vector undergoes a number of turns within a narrow area, which entails a series of very short vector segments. Since the current technology keeps the deposition flow rate constant, according to Property 2 and 4, the consecutive turns in a narrow area will generate many overfills due to frequent head speed reductions and vector geometry. Even though an overfill is preferable to underfill in building a functional part, the overfilled material will accumulate in the vicinity of the turn areas and create high bumps and a very rough surface, which may lead to more overfills in the next layer. Usually, an FD machine operator has to reduce the roller speed manually to compensate for this effect and increase the roller speed later. This manual adjustment is neither accurate nor efficient. Our proposed deposition planning approach will overcome this problem and help the operator to efficiently make a functional part of high quality.

The following rule is usually followed by an experienced FD machine operator: longer (shorter) vector segment lengths in an area require larger (smaller) flow rates in order to obtain an even layer surface for that area. The shearing effect of the nozzle will bring extra material to the neighboring areas of the turn points of long vector segments, while for short vector segments sufficient space between roads is not available to accommodate the surplus material around turn points. Therefore, our proposed approach is: (1) to assign the adjacent vector segments into groups according to the group mean; (2) to assign a flow rate or roller speed to each
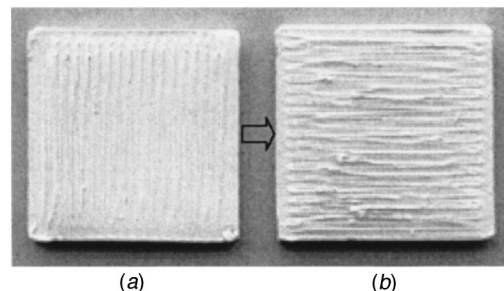

Fig. 15   Overfill correlation between two adjacent layers (*a*) current layer of part 15a (*b*) next layer of part 15b

1. $r_l := r_u$, where r_u is the upper bound of range.

2. $S :=$ set of vector segments selected from all segments in a vector according to the vector angle.

3. $T := S$, where T is the set of vector segments unselected to a group.

4. $G := \varnothing$, where G is the group being formed.

5. $s :=$ the 1st element of T in index order.

6. $T := T - \{s\}$.

7. $G := G \cup \{s\}$.

8. Is $Max(l_{ij}) - Min(l_{ij}) \leq r_k$? where $l_{ij} \in G$; k is the index for the different ranges.

    If yes,

        Is there more elements in T?

            If yes, go to step 5.

            If no, /*grouping done for r_k*/

$$\text{i. } W_k = \frac{1}{(n-g)} \sum_{i=1}^{g} \sum_{j=1}^{n_i} (l_{ij} - \bar{l}_i)^2 \ ;$$

                ii. $r_{k+1} = r_k - \varepsilon$, where ε is the step decrement;

                iii. Is $r_{k+1} \geq r_l$ where r_l is the lower bound of range.

                    If yes, go to step 2. /*grouping based on a new range*/

                    If no, /*grouping done for all r_k*/

                        i. select the r that leads to the minimum W,

$$\text{where } r \in \bigcup_k \{r_k\}, \ W \in \bigcup_k \{W_k\} \ ;$$

                        ii. select the corresponding grouping results;

                        iii. go to step 9.

    If no, /*A new group was generated.*/

        i. $T := T \cup \{s\}$.

$$\text{ii. } \bar{l}_i := \frac{\sum_{j=1}^{n_i} l_{ij}}{n_i} \ .$$

        iii. go to step 4.

9. $f_i = m(\bar{l}_i)$ $i \in [1, g]$, where g is the number of group.

Fig. 16 Grouping and mapping algorithm

group based on the group mean, using linearized mapping functions. Since roller speed is under direct control, we will assign roller speed instead of flow rate to each group.

3.2 Grouping and Mapping Algorithm. We will consider only the vector segments for the purpose of grouping, while ignoring the turn segments because their length variations are usually small compared to that of the vector segments. The straightforward way is to form a single-member group, i.e. each group contains only one vector segment. Since a roller speed is assigned to each group (each vector segment for this case), the roller reference speed has to change once the vector segment switches from one to another. This is not feasible because: (1) Flow rate will not immediately follow the change of roller speed due to the extrusion delay [23]. To compensate for this delay, we have to assign a forward-shifted roller speed to each vector segment. This will be difficult (if not impossible) to implement. (2) The small vector segments undergo acceleration and deceleration for most of time. They need a lower roller speed whose variation is unnecessary for a group of neighboring vector segments with similar lengths. Since we want to achieve average layer evenness, we choose a more practical approach, i.e. dividing the vector segments with similar lengths into groups and assigning the proper roller speeds
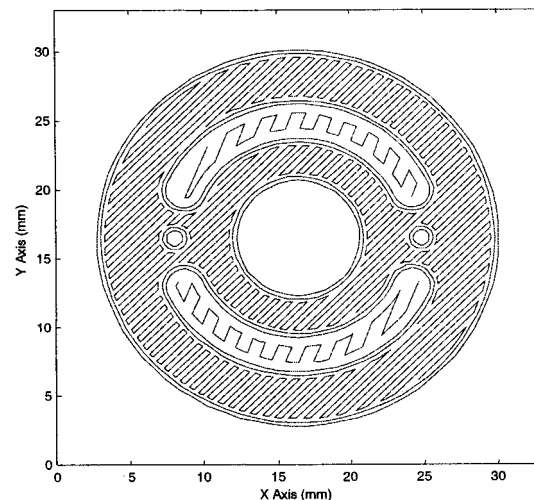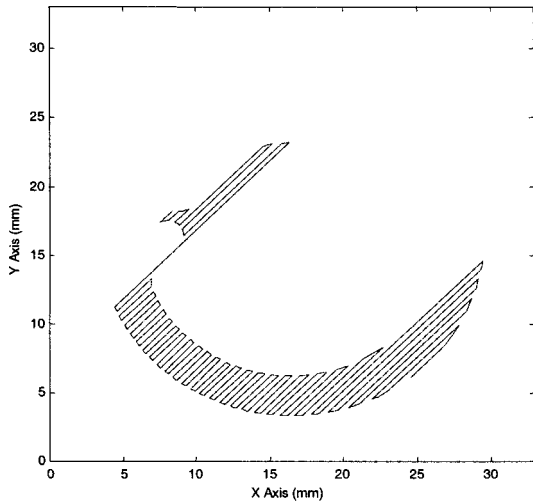

Fig. 17 Tool path of a layer

Fig. 18 A vector from Fig. 17

to them based on their mean lengths.

To group vector segments, a range r for a vector is defined by

$$r = \max_{1 \leq j \leq n_i} (l_{ij}) - \min_{1 \leq j \leq n_i} (l_{ij}) \quad i \in [1,g] \quad (3)$$

where l_{ij} is the jth vector segment in the ith group, n_i is the vector segment number of the ith group, and g is the group number of a vector. r is a measure of the similarity between vector segments within a group defined in terms of their lengths. If r is small, then fewer vector segments are in each group, i.e. more groups will be formed, and the flow rate has to be modified more frequently. On the other hand, if r is large, then fewer groups will be formed, and the flow rate is changed less frequently, but too much variation will exist in a given group. To assign an appropriate flow rate to a group, every member in a group should be somewhat similar to each other in length. So, r cannot be arbitrarily large. The selection of r for a vector can be formulated as an optimization problem [24], which is shown by

$$\min W = \frac{1}{(n-g)} \sum_{i=1}^{g} \sum_{j=1}^{n_i} (l_{ij} - \bar{l}_i)^2 \quad (4)$$

$$\text{s.t.} \quad r_l \leq r \leq r_u$$

where W is within group sum-of-square; $\bar{l}_i = \sum_{j=1}^{n_i} l_{ij}/n_i$, the mean of vector segments within a group; n is the total number of vector segments; r_l and r_u are the lower bound and the upper bound of the range respectively. The goal of this minimization is to determine r, which is the criteria to form the group.

The group mean can be mapped to the roller speed using

$$f_i = m(\bar{l}_i) \quad i \in [1,g] \quad (5)$$

where $m(.)$ is a mapping function. The mapping function can be obtained by finding the one to one relationship between group mean and flow rate through experiments. Since this function will be nonlinear, it can be represented by different linear functions for different intervals, so-called interval linearization, i.e. $m(\bar{l}_i)$ consists of a set of linear functions,

$$m(\bar{l}_i) = \{\alpha_k \bar{l}_i + \beta_k, \quad L_{k-1} \leq \bar{l}_i < L_k\} \quad (6)$$

where k is the index of intervals; α_k and β_k are coefficients; L_k is the break point for intervals.

The grouping and mapping algorithm is presented via Fig. 16, in which step 1 to 8 is for grouping while step 9 is for mapping. To illustrate this algorithm, we take a vector (see Fig. 18) from Fig. 17 as a sample [25], in which total point number = 142 and n

=57. The grouped result is shown in Fig. 19 with the group means shown in Fig. 20. In Fig. 19, nine groups are generated ($g = 9$) with $r = 2.413$ mm for the vector in Fig. 18. We can see that the adjacent vector segments of similar lengths are grouped together, while a significant difference exists between two adjacent groups.

4 Implementation of Proposed Approach

The proposed grouping and mapping algorithm is implemented in the FDMM (Fused Deposition of Multiple Materials) machine [2]. Specifically, it works as an independent module and is embedded into the CAD/CAM working procedure (see Fig. 21). After slicing and tool path generation, roller speeds are assigned to the different groups of vector segments and they are combined with the originally assigned process parameters before the procedure enters the step of FD process control and monitoring. For the details of FDMM machine, refer to [2].

The coefficients (α_k and β_k) in mapping function (6) have to be obtained through experiments. We assume 508 μm (20 mil) nozzle size, 559 μm (22 mil) road width, 254 μm (10 mil) layer thickness, 76 μm (3 mil) offset and 12.7 mm/s head speed to be constant design and process parameters. The square or rectangular parts are designed in order to keep the uniform vector segment length in each part. We obtained the relationship between vector segment length and roller speed (see Table 1 and Fig. 22) by building parts using a filament with 52.5 vol. % lead zirconate titanate (PZT) powder in 47.5 vol. % ECG 9 polymer. Choosing roller speeds according to the relationship shown in Table 1 ensures desirable layer evenness for the specific vector segment groups of those assumed parameters. We may use the vector segment lengths given in Table 1 as the break points of length intervals. Using those values of vector segment length and roller speed, α_k and β_k in mapping function (6) are derived for each linearized interval (see Table 2) according to $\alpha_k = (r_k - r_{k+1})/(l_{k+1} - l_k)$ and $\beta_k = (l_{k+1}r_k - l_k r_{k+1})/(l_{k+1} - l_k)$, where
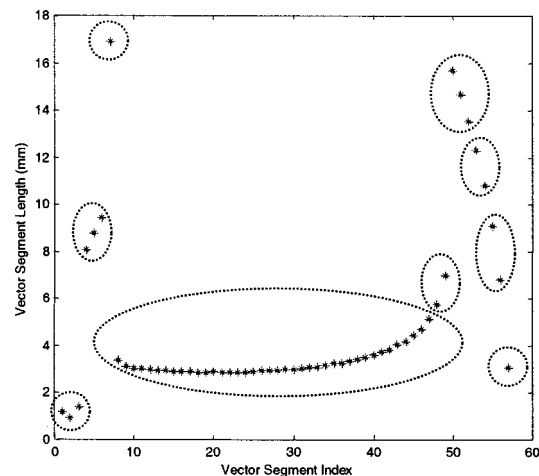

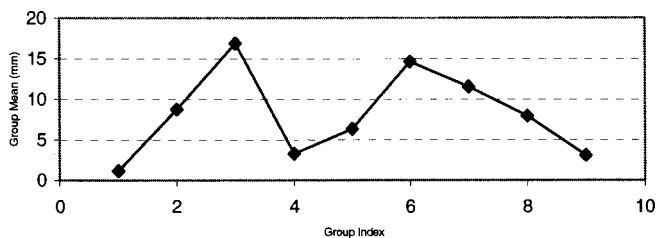**Fig. 19 Grouping result for the vector in Fig. 18**

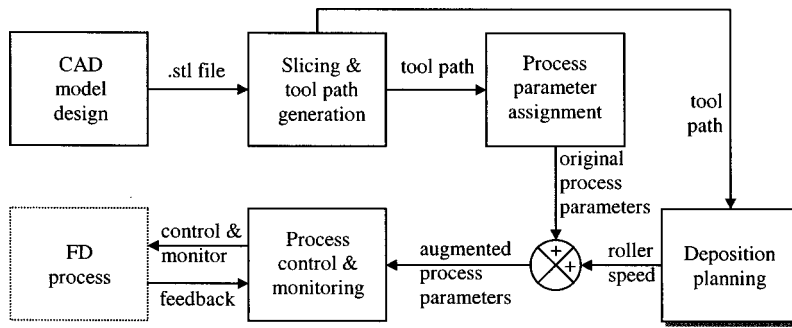

Fig. 20 Group means in Fig. 19

Fig. 21 CAD/CAM procedure with deposition planning in FD process

Table 1 Relationship between vector segment length and roller speed

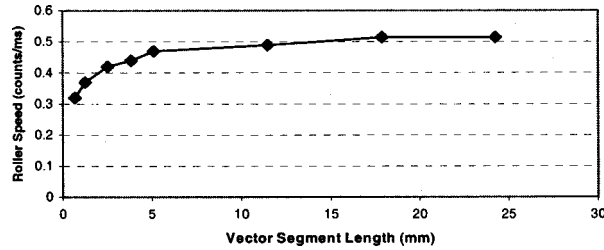| Index	1	2	3	4	5	6	7	8
Part Size (mm)	25.40× 25.40	19.05× 19.05	12.70× 12.70	6.35× 19.05	5.08× 19.05	3.81× 19.05	2.54× 19.05	1.905× 19.05
Vector Segment Length (mm)	24.232	17.882	11.494	5.105	3.835	2.522	1.285	0.660
Roller Speed (counts/ms)	0.515	0.515	0.49	0.470	0.440	0.420	0.370	0.320

Fig. 22 Nonlinear relationship between vector segment length and roller speed

Table 2 Values of α_k and β_k for different intervals

k	1	2	3	4	5	6	7
Interval (mm)	[17.882, ∞)	[11.494, 17.882)	[5.105, 11.494)	[3.835, 5.105)	[2.522, 3.835)	[1.285, 2.522)	[0.660, 1.285)
α_k	0.0	0.0994	0.0795	0.6000	0.3868	1.0267	2.0325
β_k	0.5150	0.4450	0.4540	0.3494	0.3816	0.3180	0.2672

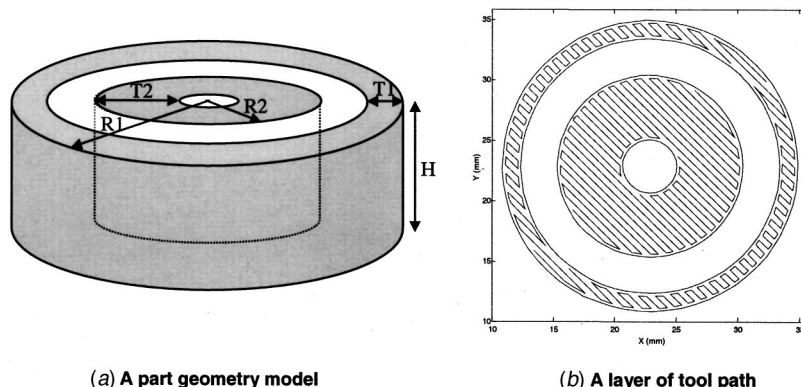(a) A part geometry model   (b) A layer of tool path

Fig. 23 A piezoelectric actuator part designed for testing proposed approach
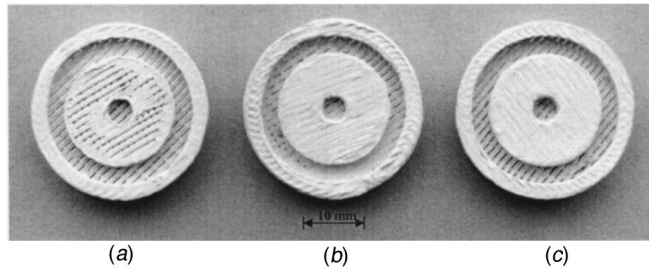
Fig. 24 Built green parts with removable base using different methods constant roller speed (0.38 counts/ms) (*b*) constant roller speed (0.48 counts/ms) (*c*) deposition planning (using varying roller speeds)

Table 3 Comparison of geometric parameters for designed and built parts

Geometric parameters		R1	T1	R2	T2
Designed part (mm)		12.192	2.032	7.620	6.096
Built part variance (%)	Constant roller Speed = 0.38 counts/ms	-0.42	-3.38	-1.33	-0.26
	Constant roller Speed = 0.48 counts/ms	1.85	11.25	2.87	1.90
	Deposition planning	-0.04	1.25	0.33	0.20

Table 4 Comparison of the deviations from the plane for the built parts

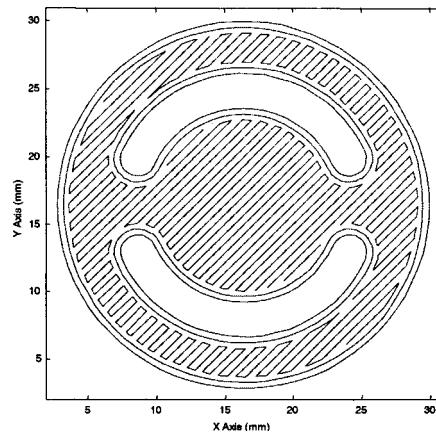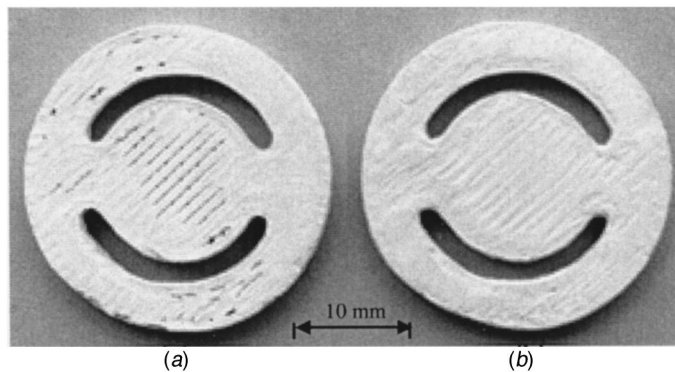| Maximum heights	Overfill (mm)	Underfill (mm)
Constant roller speed = 0.38 counts/ms	0.069	>0.5
Constant roller speed = 0.48 counts/ms	0.173	0.0
Deposition planning	0.037	0.0

Fig. 25 A layer of tool path for second part

Fig. 26 A structural component using two different methods (*a*) with constant roller speed (0.41 counts/ms) (*b*) using deposition planning approach

$k \in [1,7]$; r_k and l_k are roller speed and vector segment length respectively. We assume all the vector segment lengths are longer than 660 μm, which is physically applicable.

To demonstrate the feasibility of the proposed deposition planning method, a piezoelectric actuator part and a structural piezoelectric component are designed using QuickSlice© and built with PZT in FDMM machine. For the first part, the designed geometry model and one sample layer are shown in Fig. 23. This part consists of two coaxial hollow cylinders, in which R1 = 12.192 mm, R2 = 7.620 mm, T1 = 2.032 mm, T2 = 6.096 mm and H = 10.160 mm. The exterior wall thickness (T1) is much thinner than that of the interior one (T2). Within one layer, most of the vectors in the exterior ring are much shorter than those in the interior one. To compare the proposed approach to the constant flow rate approach (used in current FD technology), we built three green parts based on the same model (in Fig. 23) with varying roller speeds and two different constant roller speeds, 0.38 and 0.48 counts/ms respectively (see Fig. 24, counts/ms is the unit of roller speed). The parameters for tool path and build process are chosen the same as those used in experiments for deriving Table 1, because we may use the linearized mapping functions of α_k and β_k listed in Table 2. The key geometric parameters for the designed and built parts are listed in Table 3 for comparison. The maximum overfill and underfill heights of the built parts are given in Table 4. These results indicate that: (1) Inappropriate roller speed leads to (in-plane and out-of-plane) dimensional inaccuracy and a large variance. Since the exterior ring is narrower than the interior one, lower roller speed is preferable for the exterior ring to the interior one. (2) Constant flow rate will not satisfy the layer evenness requirement for the various geometries in a layer. Although a (nearly) suitable constant roller speed for building an accurate geometry can be found, e.g. 0.38 counts/ms for this part, it does not meet the layer evenness requirement within a deposition area for more complex geometries. In Fig. 23(a), we can see that many voids occur in the interior ring. A larger flow rate (e.g. 0.48 count/ms) may remove the voids in the interior ring, while it is likely to cause many overfills in the outer ring. (3) Varying flow rates (or roller speed) due to deposition planning successfully overcomes the geometric complexity of a layer and creates the satisfactory layer evenness. In Tables 3 and 4, we note that among the three methods, the highest accuracy is achieved via the deposition planning approach.

For the second test part, one sample layer of the designed tool path is shown in Fig. 25. This part consists of two connected concentric cylinders. Since most of the area in the outer ring is filled by short vector segment lengths, to ensure dimensional accuracy, the lower roller speed (0.41 counts/ms) is selected for the part in Fig. 26(a). However, most of the area in the inner cylinder is underfilled. In contrast to the part in Fig. 26(a), a fully dense part was made using deposition planning approach (see Fig. 26(b)). This result further demonstrates the effectiveness of the proposed planning approach.

5 Conclusion and Future Research

Current FD technology applies constant deposition flow rate, which cannot meet the requirement for building functional parts due to the varying geometric complexity within a layer. To achieve a desirable layer evenness of a functional part, we performed an overfill and underfill analysis for the FD processes and identified five important properties of the FD processes that contribute to part quality. According to the underfill and overfill analysis, a deposition planning approach based on a grouping and mapping algorithm was proposed. The main idea is to group the adjacent vector segments according to their similarities and assign an appropriate flow rate (or roller speed) to each group using linearized mapping functions. The mapping functions for a class of parts of same design parameters have to be obtained experimentally through building the specially designed parts of those parameters, e.g. nozzle size, offset value, road width. Finally, two piezoelectric parts were designed and built to demonstrate the effectiveness and feasibility of the proposed approach in achieving good quality of functional parts. The proposed approach is applicable to FDC, FDMM, and FDMet processes.

One of the functions realized by the proposed grouping and mapping algorithms is to adjust the roller speed to compensate for the speed reductions at head turn points according to Property 1 and 2. According to Eq. (2), one direct approach is to measure the head speed in real time and multiply it by a transfer function (digital controller) as a reference to the roller speed. Theoretically, the road geometry should be kept constant by this way. We are studying this real time control approach and will compare it to the off-line planning approach proposed in this paper.

Appendix

Proof of Property 2:
Assume $\mathbf{V}_1$ and $\mathbf{V}_2$ are speed vectors before and after turn points respectively (see Fig. 5), for a blended-move at a turn, velocity change in X axis and Y axis takes the same amount of time T and the (reference) acceleration or deceleration keeps unchanged during a turn. We prove in two cases the first part of the statement, i.e. table speed of blended-move during turn period is less than V_0.

Case 1: after one turn point, the object can accelerate to V_0 before reaching the next turn point. Assuming V_x and V_y are object velocities along X and Y axes, we have

$$V_x = V_1 \cos(\alpha_1)(1-\lambda) + V_2 \cos(\alpha_2)\lambda \qquad (7)$$

$$V_y = V_1 \sin(\alpha_1)(1-\lambda) + V_2 \sin(\alpha_2)\lambda \qquad (8)$$

where $\lambda = t/T$, $0 \leq t \leq T$. The square of turn speed is

$$V^2 = V_x^2 + V_y^2 = V_1^2(1-\lambda^2) + V_2^2\lambda^2 + 2V_1V_2\lambda(1-\lambda)\cos(\alpha_1-\alpha_2) \qquad (9)$$

since $-1 \leq \cos(\alpha_1-\alpha_2) \leq 1$, $V_1 = V_2 = V_0 > 0$, $0 \leq \lambda \leq 1$, we have

$$V^2 \leq V_1^2(1-\lambda)^2 + V_2^2\lambda^2 + 2V_1V_2\lambda(1-\lambda) = V_0^2 \qquad (10)$$

When $\alpha_1 = \alpha_2$, the equal relationship holds in Eq. (10), i.e. V $< V_0$ for turn period, in which $\alpha_1 \neq \alpha_2$.

Case 2: after one turn point, the object cannot accelerate to V_0 when reaching next turn point.
Assume the object accelerates to V_2' ($<V_2$) when reaching next turn point, similar to Eq. (9), the turn speed becomes

$$V^2 = V_1^2(1-\lambda)^2 + V_2'^2\lambda^2 + 2V_1V_2'\lambda(1-\lambda)\cos(\alpha_1-\alpha_2) \qquad (11)$$

since $-1 \leq \cos(\alpha_1-\alpha_2) \leq 1$, $V_1 = V_2 = V_0 > V_2' > 0$, $0 \leq \lambda \leq 1$, we have

$$V^2 \leq V_1^2(1-\lambda)^2 + V_2'^2\lambda^2 + 2V_1V_2'\lambda(1-\lambda) < V_0^2 \qquad (12)$$

i.e. V $< V_0$ for the turn period.
Now, we prove the second part of the statement. It is easy to see that $\alpha_1 - \alpha_2 \in [-\pi, \pi]$. The more acute the turn angle is, the nearer $\alpha_1 - \alpha_2$ is to $-\pi$ or π. Since $\cos(\alpha_1-\alpha_2)$ is monotone decreasing either from 0 to π or from 0 to $-\pi$, and $V_1 > 0$, $V_2 > 0$, $0 \leq \lambda \leq 1$, according to Eq. (9), we know that the more acute the turn angle is, the more reduction of velocity (V) occurs during the turn period.
Q.E.D.

Proof of Property 3:
For a stop-at-turn scheme, AO = V_1T/2, OB = V_2T/2, where O is the turn point. According to Cosine theorem, we have

$$AB^2 = \left(\frac{V_1 T}{2}\right)^2 + \left(\frac{V_2 T}{2}\right)^2 - 2\left(\frac{V_1 T}{2}\right)\left(\frac{V_2 T}{2}\right)\cos(\pi - \alpha_1 + \alpha_2)$$

$$= \frac{T^2}{4}(V_1^2 + V_1^2 + 2V_1 V_2 \cos(\alpha_1 - \alpha_2)) \qquad (13)$$

where $\alpha_1 > 0$ and $\alpha_2 > 0$.

For a blended move, the displacement along X axis at time T is

$$D_x = \frac{(V_{1x} + V_{2x})T}{2} = \frac{(V_1 \cos(\alpha_1) + V_2 \cos(\alpha_2))T}{2} \qquad (14)$$

The displacement along Y axis at time T is

$$D_y = \frac{(V_{1y} + V_{2y})T}{2} = \frac{(V_1 \sin(\alpha_1) + V_2 \sin(\alpha_2))T}{2} \qquad (15)$$

The square of the combined displacement at time T is

$$D^2 = D_x^2 + D_y^2 = \frac{T^2}{4}(V_1^2 + V_2^2 + 2V_1 V_2 \cos(\alpha_1 - \alpha_2)) \qquad (16)$$

Hence, $AB^2 = D^2$. It is easy to see that the point B is the location where the blended move ends.
Q.E.D.

Proof of Property 4:
The shaded area in Fig. 7 is

$$S_{\text{overfill}} = \frac{W^2}{4}\left(\cot\left(\frac{\theta}{2}\right) + \frac{\theta}{2} - \frac{\pi}{2}\right) \qquad (17)$$

Since $cot(\theta/2)$ is monotone decreasing when $0 \leq \theta \leq \pi$, S_{overfill} is increasing while θ is decreasing. $MaxS_{\text{overfill}} = \infty$ when $\theta = \pi$, $MinS_{\text{overfill}} = 0$ when $\theta = 0$. $S_{overfill}$ is proportional to w^2 for a specific θ.
Q.E.D.

Proof of Property 5:
In Fig. 10, since $S_1 = S_2 + S_3$, the area of the rectangle ABCD is equal to the area of two semi-circles or a complete circle. Hence, we have

$$t(t + f^*) = \frac{\pi t^2}{4} \qquad (18)$$

where f^* is the desired (negative) offset in the statement. Solve Eq. (18), we get

$$f^* = \frac{(\pi - 4)t}{4} \qquad (19)$$

Q.E.D.

References

[1] Danforth, S. C., Agarwala, M., Bandyopadhyay, A., Langrana, N. A., Jamalabad, V. R., Safari, A., and van Weeren, R., 1998, "Solid Freeform Fabrication Methods," U.S. Patent no. 5,738,817.

[2] Jafari, M. A., Han, W., Mohammadi, F., Safari, A., Danforth, S. C., and Langrana, N. A., 2000, "A Novel System for Fused Deposition of Advanced Multiple Ceramics." Rapid Prototyping Journal, **6**, No. 3, pp. 161–174.

[3] Agarwala, M. K., van Weeren, R., Bandyopadhyay, A., Whalen, P. J., Safari, A., and Danforth, S. C., 1996, "Fused Deposition of Ceramics and Metals: An Overview," *Proceedings of Solid Freeform Fabrication Symposium*, Austin, TX, pp. 385–390.

[4] Agarwala, M. K., Jamalabad, V. R., Langrana, N. A., Safari, A., Whalen, P. J., and Danforth, S. C., 1996, "Structural Quality of Parts Processed by Fused Deposition," Rapid Prototyping Journal, **2**, No. 4, pp. 4–19.

[5] Safari, A., 1999, "Novel Piezoelectric Ceramics and Composites for Sensors and Actuators Applications," Mater. Res. Innovations, **2**, pp. 263–269.

[6] Wu, G., Langrana, N. A., Rangarajan, S., McCuiston, R., Sadanji, R., Danforth, S. C., and Safari, A., 1999, "Fabrication of Metal Components using FDMet: Fused Deposition of Metals," *Proceedings of Solid Freeform Fabrication Symposium*, Austin, TX.

[7] Kattethota, G., and Henderson, M., 1998, "A Visual Tool to Improve Layered Manufacturing Part Quality," *Proceedings of Solid Freeform Fabrication Symposium*, Austin, TX, pp. 327–334.

[8] Jamalabad, V. R., Agarwala, M. K., Langrana, N. A., and Danforth, S. C., 1996, "Process Improvements in Fused Deposition of Ceramics (FDC): Progress Towards Structurally Sound Components," *Proceedings of the 1996 ASME Design Engineering Technical Conference and Computers in Engineering Conference*, Irvine, CA, pp. 1–8.

[9] Kao, J.-H., and Prinz, F. B., 1998, "Optimal Motion Planning for Deposition in Layered Manufacturing," *Proceedings of 1998 ASME Design Engineering Technical Conferences*, Atlanta, GA, Sept. pp. 1–20.

[10] Kulkarni, P., and Dutta, D., 1995, "Adaptive Slicing of Parametrizable Algebraic Surfaces for Layered Manufacturing," *21st Annual Design Automation Conference, ASME, Design Engineering Division* (Publication), DE-Vol. 82, No. 1, pp. 211–217.

[11] Allen, S. W., and Dutta, D., 1995, "Determination and Evaluation of Support Structures in Layered Manufacturing," Journal of Design and Manufacturing, **5**, pp. 153–162.

[12] Agarwala, M. K., Bandyopadhyay, A., van Weeren, R., Safari, A., Danforth, S. C., Langrana, N. A., Jamalabad, V. R., and Whalen, P. J., 1996, "FDC, Rapid Fabrication of Structural Components," Am. Ceram. Soc. Bull. , **75**, No. 11, pp. 60–65.

[13] Comb, J. W., Priedeman, W. R., and Turley, P. W., "Layered Manufacturing Control Parameters and Material Selection Criteria," Manufacturing Science and Engineering, ASME, Production Engineering Division (Publication) **68-2**, pp. 547–556.

[14] Bouhal, A., Jafari, M. A., Han, W., and Fang, T., 1999, "Tracking Control and Trajectory Planning in Layered Manufacturing Applications," IEEE Trans. Ind. Electron., **46**, No. 2, pp. 445–451.

[15] Kulkarni, P., and Dutta, D., 1999, "Deposition Strategies and Resulting Part Stiffness in Fused Deposition Modeling," ASME J. Manuf. Sci. Eng., **121**, Feb. pp. 93–103.

[16] Yardimci, M. A., Guceri, S. I., Agarwala, M. K., and Danforth, S. C., 1996, "Part Quality Prediction Tools for Fused Deposition Processing," *Proceedings of Solid Freeform Fabrication Symposium*, Austin, TX, pp. 539–548.

[17] Marsan, A. L., Allen, S., Kulkarni, P., and Dutta, D., 1996, "An Integrated Software System for Process Planning for Layered Manufacturing," *Proceedings of Solid Freeform Fabrication Symposium*, Austin, TX, pp. 661–668.

[18] van Weeren, R., Agarwala, M. K., Jamalabad, V. R., Bandyopadhyay, A., Langrana, N. A., Safari, A., Whalen, P., Danforth, S. C., and Ballard, C., 1995, "Quality of Parts Processed by Fused Deposition," *Proceedings of Solid Freeform Fabrication Symposium*, Austin, TX.

[19] Kao, J.-H., and Prinz, F. B., 1998, "Optimal Motion Planning for Deposition in Layered Manufacturing," *Proceedings of 1998 ASME Design Engineering Technical Conferences*, Atlanta, GA, Sept. pp. 1–20.

[20] Qiu, D., Langrana, N. A., Danforth, S. C., Jafari, M. A., and Safari, A., 1998, "Development of Multimaterial Virtual Layered Manufacturing Simulation," *Proceedings of Third Pacific Rim International Conference on Advanced Materials and Processing*, July, pp. 1625–1630.

[21] Yan, X., and Gu, P., 1996, "A Review of Rapid Protyping Technologies and Systems," Comput.-Aided Des., **28**, No. 4, pp. 307–318.

[22] Delta Tau Data Systems Inc., PMAC User's Manual, 1996 version 1.6.

[23] Bertoldi, M., 1998 "From Rapid Prototyping to Rapid Manufacturing: Analysis of The Fused Deposition Process," M. S. Thesis, The University of Illinois at Chicago.

[24] Everitt, B. S., 1993, *Cluster Analysis*, 3rd ed., Halsted Press.

[25] Dai, C., Qi, G., Rangarajan, S., Langrana, N. A., Safari, A., and Danforth, S. C., 1997, "High Quality, Fully Dense Ceramic Components Manufactured Using Fused Deposition of Ceramics (FDC)," *Proceedings of Solid Freeform Fabrication Symposium*, Austin, TX.